



# Humanization of the entire murine *Mapt* gene provides a murine model of pathological human tau propagation

Received for publication, May 22, 2019, and in revised form, June 27, 2019. Published, Papers in Press, July 4, 2019, DOI 10.1074/jbc.RA119.009487

✉ Takashi Saito<sup>‡§1</sup>, Naomi Mihira<sup>‡</sup>, Yukio Matsuba<sup>‡</sup>, Hiroki Sasaguri<sup>‡</sup>, ✉ Shoko Hashimoto<sup>‡</sup>, Sneha Narasimhan<sup>¶</sup>, Bin Zhang<sup>¶</sup>, Shigeo Murayama<sup>||</sup>, Makoto Higuchi<sup>\*\*</sup>, Virginia M. Y. Lee<sup>¶</sup>, John Q. Trojanowski<sup>¶</sup>, and Takaomi C. Saïdo<sup>+2</sup>

From the <sup>‡</sup>Laboratory for Proteolytic Neuroscience, RIKEN Center for Brain Science, 2-1 Hirosawa, Wako-city, Saitama 351-0198, Japan, the <sup>§</sup>Department of Neuroscience and Pathobiology, Research Institute of Environmental Medicine, Nagoya University, Nagoya, Aichi 464-8601, Japan, the <sup>¶</sup>Department of Pathology and Laboratory Medicine, Institute on Aging and Center for Neurodegenerative Disease Research, University of Pennsylvania School of Medicine, Philadelphia, Pennsylvania 19104, the <sup>||</sup>Department of Neuropathology, Tokyo Metropolitan Geriatric Hospital, 35-2 Sakaecho, Itabashi, Tokyo 173-0015, Japan, and the <sup>\*\*</sup>Department of Functional Brain Imaging Research, National Institute of Radiological Sciences, National Institutes for Quantum and Radiological Science and Technology, Chiba 263-8555, Japan

Edited by Paul E. Fraser

In cortical regions of brains from individuals with preclinical or clinical Alzheimer's disease (AD), extracellular  $\beta$ -amyloid ( $A\beta$ ) deposition precedes the aggregation of pathological intracellular tau (the product of the gene microtubule-associated protein tau (*MAPT*)). To our knowledge, current mouse models of tauopathy reconstitute tau pathology by overexpressing mutant human tau protein. Here, through a homologous recombination approach that replaced the entire murine *Mapt* gene with the human ortholog, we developed knock-in mice with humanized *Mapt* to create an *in vivo* platform for studying human tauopathy. Of note, the humanized *Mapt* expressed all six tau isoforms present in humans. We next cross-bred the *MAPT* knock-in mice with single amyloid precursor protein (*App*) knock-in mice to investigate the  $A\beta$ -tau axis in AD etiology. The double-knock-in mice exhibited higher tau phosphorylation than did single *MAPT* knock-in mice but initially lacked apparent tauopathy and neurodegeneration, as observed in the single *App* knock-in mice. We further observed that tau humanization significantly accelerates cell-to-cell propagation of AD brain-derived pathological tau both in the absence and presence of  $A\beta$ -amyloidosis. In the presence of  $A\beta$ -amyloidosis, tau accumulation was intensified and closely associated with dystrophic neurites, consistently showing that  $A\beta$ -amyloidosis affects tau

pathology. Our results also indicated that the pathological human tau interacts better with human tau than with murine tau, suggesting species-specific differences between these orthologous pathogenic proteins. We propose that the *MAPT* knock-in mice will make it feasible to investigate the behaviors and characteristics of human tau in an animal model.

Alzheimer's disease (AD)<sup>3</sup> is the primary cause of dementia in the elderly and imposes a social and economic burden on modern society. In cortical regions of the preclinical and clinical AD brains, extracellular  $A\beta$  deposition precedes the aggregation of pathological intracellular tau (*MAPT* gene product). These aggregates, composed of hyperphosphorylated tau, form in the brain and are followed by irreversible progressive neurodegeneration. This pathological chronology agrees with the cause-and-effect relationship proposed by the amyloid cascade hypothesis (1–3).

Despite current knowledge, the molecular mechanisms by which  $A\beta$  deposition induces the formation of neurofibrillary tangles (NFTs) remain elusive. We believe that this is in part caused by a lack of relevant animal models. Accordingly, we demonstrated nonphysiological aspects of the existing models in our previous studies (4–6), with the major problem being that these models overexpress mutant amyloid precursor protein (APP) and/or presenilin-1 (PS1) and tau. Of particular note, *MAPT* gene mutations are known to cause frontotemporal dementia with Parkinsonism linked to chromosome 17 (FTDP-17), but not AD, thus calling into question the relevance of using mutant tau-overexpressing mice in AD research. Nevertheless, tau mutations can be considered as relevant tauopa-

This work was supported in part by research grants from the RIKEN Center for Brain Science, research grants from the RIKEN Aging Project, a Grant-in-Aid-for Scientific Research (B) from MEXT (to T. S.), Precursory Research for Embryonic Science and Technology from JST (to T. S.), the Cell Science Research Foundation (to T. S.), the Brain Mapping by Integrated Neurotechnologies for Disease Studies (Brain/MINDS) from the Japan Agency for Medical Research and Development (AMED) (Grant JP18dm027001) (to T. C. S.), Astellas Pharma, Inc. JSPS KAKENHI Grant JP16H06277 (to S. M.), and National Institutes of Health Grants AG10124 and AG17586 (to V. M. Y. L. and J. Q. T.). T. S., Y. M., S. H., and T. C. S. serve as advisor, director, researcher, and CEO, respectively, for RIKEN BIO Co. Ltd., which sublicenses animal models, *App* KI mice, to for-profit organizations, the proceeds from which are used for the identification of disease biomarkers. The content is solely the responsibility of the authors and does not necessarily represent the official views of the National Institutes of Health.

This article contains Fig. S1.

<sup>1</sup> To whom correspondence may be addressed. E-mail: [takashi.saito.aa@riken.jp](mailto:takashi.saito.aa@riken.jp).

<sup>2</sup> To whom correspondence may be addressed. E-mail: [saido@brain.riken.jp](mailto:saido@brain.riken.jp).

<sup>3</sup> The abbreviations used are: AD, Alzheimer's disease;  $A\beta$ , amyloid  $\beta$ ; APP, amyloid precursor protein; FTDP-17, frontotemporal dementia with Parkinsonism linked to chromosome 17; KI, knock-in; dKI, double knock-in; LLPS, the liquid-liquid phase separation; PS1, presenilin-1; NFT, neurofibrillary tangle; 3R and 4R, three- and four-repeat, respectively; GuHCl, guanidine HCl; KO, knockout; ANOVA, analysis of variance; GAPDH, glyceraldehyde-3-phosphate dehydrogenase.

thy-accelerating factors if they are used in a nonoverexpression paradigm.

To overcome these drawbacks, we have created novel A $\beta$ -amyloidosis models, using a knock-in (KI) strategy and reported the advantages of KI models over the overexpression models (5, 7). However, we did not observe NFTs in these mice during their lifespan. One possible explanation for this is that murine tau might be incompatible for NFT formation, presumably due to differences in the isoform expression profile between humans and mice (8, 9). In the present study, we have created mutant mice in which the murine *Mapt* gene, including all exons and introns, are humanized (*MAPT* KI mice) to overcome the above concern. These mice express all six isoforms of tau in a manner similar to that in humans; in contrast, normal adult mouse brains express only the three four-repeat (4R) tau isoforms (8). Tau proteins in the KI mice show normal axonal localization, unlike that in tau-overexpressing mice (10). When we cross-bred the *MAPT* KI mice with single *App* KI mice (*App*<sup>NL-G-F</sup> mice), we confirmed that the double knock-in (dKI) mice exhibited pathological and cognitive features similar to those of single *App*<sup>NL-G-F</sup> mice. These observations indicate that human tau in the mouse brain plays physiological and pathological roles essentially identical to those of murine tau, suggesting that tau humanization does not cause any artificial phenotypes in these mice.

One of the characteristic features of pathological tau is that it propagates from neuron to neuron in the brain (11). This may explain aging-associated expansion of tau pathology described by Braak and Braak (12). Recently, He *et al.* (13) demonstrated that presence of the A $\beta$  plaque milieu was linked to accelerated propagation of pathological tau particularly in association with dystrophic plaque-associated neurite formation. We thus analyzed the difference in tau propagation between WT and human *MAPT* KI mice. We were surprised to see that humanization of murine tau significantly accelerated propagation of pathological tau in the presence and absence of A $\beta$ -amyloidosis. Apparently, the pathological human tau interacted better with normal human tau than with murine tau in the human *MAPT* KI mice. These results suggest the presence of species-defined preference between human *versus* mouse tau proteins. The divergence may be attributed to the differences in the amino acid sequences and in the alternative splicing-dependent isoform expression (14). The *MAPT* KI mice will serve as a valuable platform for creating a relevant model(s) of FTDP-17 using genome-editing technology (15).

## Results

### Characterization of human *MAPT* KI mice

Normal adult human brains express six distinct isoforms of tau generated by alternative splicing (14). They are classified into 3R-tau and 4R-tau, depending on the number of repeated microtubule-binding domains (3 repeats in 3R and 4 in 4R). Importantly, NFTs in human AD comprise an equal mixture of all 3R and 4R tau isoforms (14). In contrast, 4R-tau aggregates may cause corticobasal degeneration or progressive supranuclear palsy, whereas deposition of 3R-tau aggregates characterize Pick's disease (14, 16).

The major difference between tau isoforms present in adult mouse and human brains is that the former possesses 4R-tau only, although they express 3R-tau in development like humans, whereas normal adult human brains also possess 3R-tau (17). In contrast, almost all existing mouse models of tauopathy overexpress one of the six possible tau isoforms (18). These mice, with or without FTDP-17 mutations, do not fully recapitulate the pathophysiology of tauopathy. In addition, because the presence of murine tau may hamper human tau aggregation, models in which endogenous murine tau is deleted are preferred (19). Ideally, the mouse model of tauopathy should be based on the KI strategy because overexpression of tau may disturb the normal physiological functions of neurons, such as microtubule assembly and synaptic functions (20).

We therefore generated mutant mice, in which the entire murine *Mapt* gene has been humanized (*MAPT* KI mice) by homologous recombination as described (21). The tau protein in *MAPT* KI mice localized to axons (*e.g.* mossy fibers) in a manner similar to endogenous tau in WT mice (10) (Fig. 1, *A* and *B*). In clear contrast, P301S-tau transgenic mice, which express human tau protein at 5-fold higher levels than endogenous mouse tau (22) (Fig. 1*B*), exhibit an abnormal distribution of tau, such as dendritic mislocalization (23) (Fig. 1*C*). Moreover, the humanization of murine tau did not affect A $\beta$  levels in the brain (Fig. 1*D*). These observations suggest that the human tau proteins in *MAPT* KI mice are functionally, physiologically, and structurally normal and that *MAPT* KI incorporates correctly into murine neuronal systems.

### Humanization of *Mapt* gene in *App* KI mice

We next cross-bred *MAPT* KI mice with *App*<sup>NL-F</sup> and *App*<sup>NL-G-F</sup> mice (5). 6-Month-old *App*<sup>NL-G-F</sup>/*MAPT* dKI mice exhibited a significantly higher tau phosphorylation status than single *MAPT* KI mice at Ser-202/Thr-205, Ser-396/Ser-404, and Ser-422, as recognized by AT8, PHF-1, and anti-pS422 antibodies, respectively (Fig. 2, *A* and *B*). Similarly, 6-month-old single *App*<sup>NL-G-F</sup> KI mice also showed greater tau phosphorylation than WT mice in a similar manner (Fig. 2, *C* and *D*). Immunohistochemistry allowed us to detect AT8 signals in dystrophic neurites around A $\beta$  plaques, but we observed no NFTs in single *App*<sup>NL-G-F</sup> KI mice or the dKI mice, where we used P301S-tau Tg and AD brains as positive controls (Fig. 2, *E* and *F*). Humanization of the *Mapt* gene did not affect A $\beta$ -amyloid deposition, neuroinflammation (Fig. 3), or memory in *App*<sup>NL-G-F</sup> mice (Fig. S1).

At 24 months of age, *App*<sup>NL-G-F</sup>/*MAPT* dKI mice exhibited significantly higher tau phosphorylation than single *MAPT* KI mice at Ser-202/Thr-205, Ser-396/Ser-404, and Ser-422 (Fig. 4, *A* and *B*). A $\beta$ -amyloidosis accelerated phosphorylation of murine and human tau proteins to a similar extent in the *App* KI and *App*/*MAPT* dKI mice, respectively (Fig. 4, *C* and *D*), indicating that murine and human tau proteins behave comparably in terms of A $\beta$ -amyloidosis-evoked phosphorylation. We also observed that A $\beta$ -amyloidosis induced more prominent neuroinflammation in these mutant mice (21). Consistently, the single *App*<sup>NL-G-F</sup> KI and *App*<sup>NL-G-F</sup>/*MAPT* dKI mice exhibited more dystrophic neurites than the WT and single *MAPT* KI mice without NFT formation (Fig. 4, *E* and *F*).

## Humanization of murine *Mapt* gene

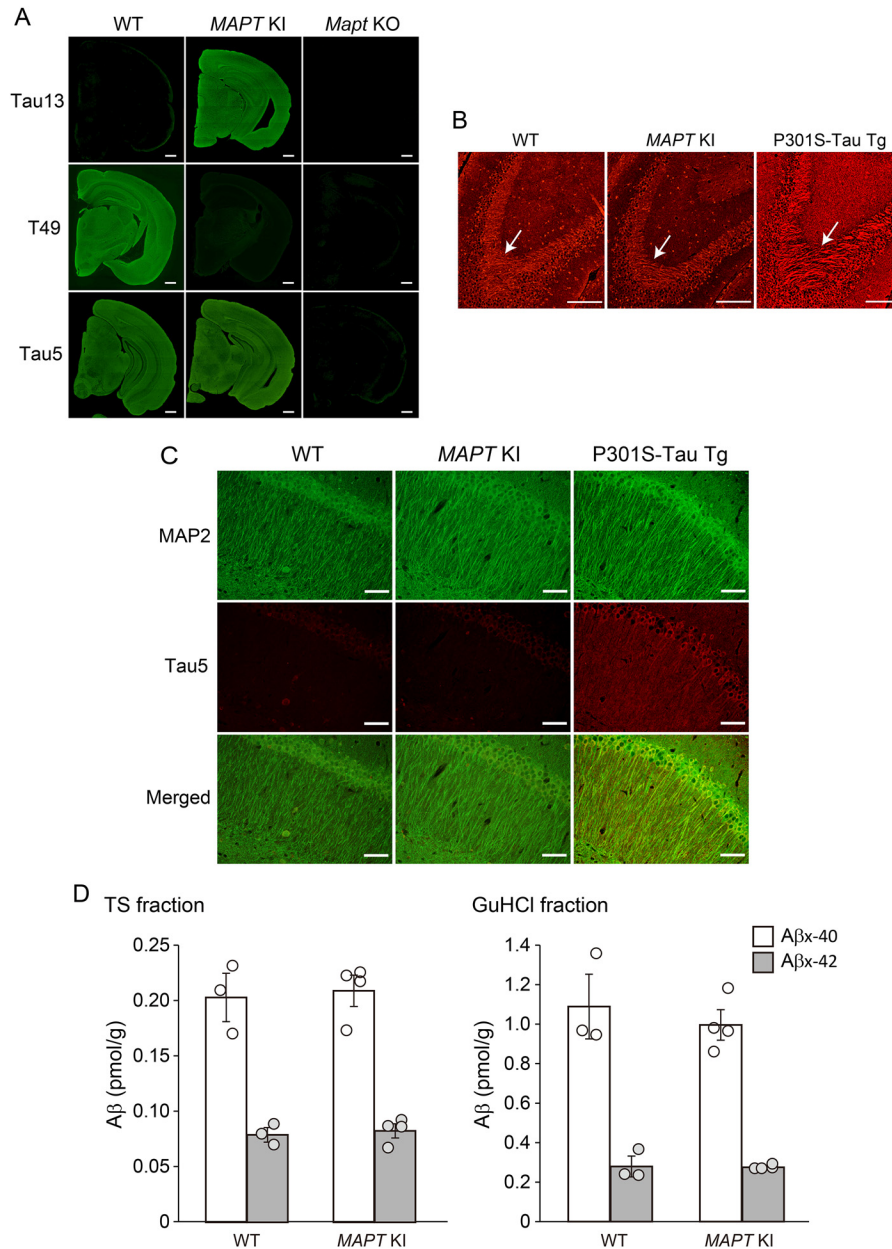


**Figure 1. Biochemical and pathological properties of tau protein in *MAPT* KI mice.** *A*, tau expression in *MAPT* KI mice was immunostained with the anti-tau antibodies Tau13, T49, and Tau5. *B*, axonal distribution of tau at mossy fiber in *MAPT* KI mouse brains. Brain sections from *MAPT* KI mice and P301S-tau transgenic mice were immunostained with the anti-pan-tau antibody, Tau1. Arrows, mossy fibers. *C*, localization of tau in *MAPT* KI brains. Brain sections from *MAPT* KI mice were doubly immunostained with Tau5 (red) and anti-MAP2 antibody as a dendritic marker (green). Scale bars, 500  $\mu$ m (*A*), 250  $\mu$ m (*B*), and 50  $\mu$ m (*C*). *D*, A $\beta$  levels in the brains of *MAPT* KI mice. Biochemical quantification of A $\beta$  in mouse brains. A $\beta$ <sub>40</sub> and A $\beta$ <sub>42</sub> in the TS and GuHCl fractions of cortical tissue from 12-month-old mouse brains were quantified by sandwich ELISA. Data represent mean  $\pm$  S.E. (error bars) ( $n = 3$  (WT) and  $n = 4$  (*MAPT* KI), Student's *t* test (TS-A $\beta$ <sub>40</sub>:  $t(5) = 0.287$ ,  $p = 0.392$ ; TS-A $\beta$ <sub>42</sub>:  $t(5) = 0.460$ ,  $p = 0.332$ ; GuHCl-A $\beta$ <sub>40</sub>:  $t(5) = 0.679$ ,  $p = 0.736$ ; GuHCl-A $\beta$ <sub>42</sub>:  $t(5) = 0.121$ ,  $p = 0.546$ )).

*App*<sup>NL-F</sup> mice exhibited a much less aggressive pathology than the *App*<sup>NL-G-F</sup> mice (5), but *App*<sup>NL-F</sup>/*MAPT* dKI mice exhibited higher tau phosphorylation than single *MAPT* KI mice (Fig. 5). Thus, both in *App*<sup>NL-F</sup> and *App*<sup>NL-G-F</sup> mice, A $\beta$ -amyloidosis augmented tau phosphorylation.

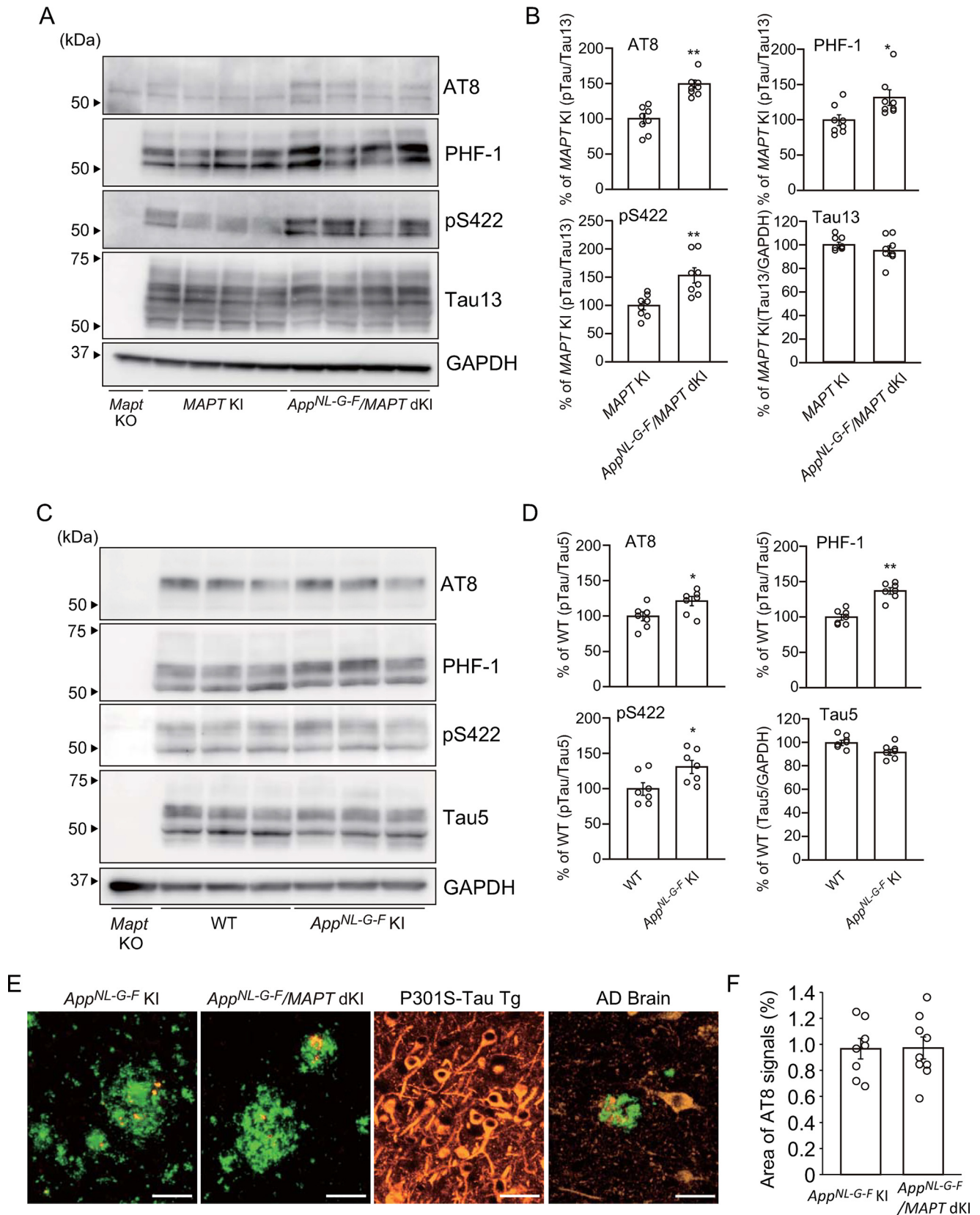
Several studies have shown an aberrant increase of exon 10-containing 4R-tau isoforms in AD and tauopathy cases (24, 25). Exon 10 encodes one of the microtubule-binding domains, and its inclusion gives rise to the production of 4R-tau. However, it has been difficult to analyze tau splicing using existing mouse models because of the lack of a suitable model express-

ing all human isoforms without overexpression of tau. To examine the contribution of A $\beta$  pathology to tau splicing, we determined the level of each tau isoform in *MAPT* KI and *App*<sup>NL-G-F</sup>/*MAPT* dKI mice. The relative expression ratio of mRNA for 4R-tau/3R-tau was almost the same between aged *MAPT* KI mice and *App*<sup>NL-G-F</sup>/*MAPT* dKI mice, with values of  $0.71 \pm 0.08$  and  $0.69 \pm 0.11$  ( $n = 4$  each), respectively, obtained for each strain (Fig. 4, *G* and *H*). The isoform profile of tau protein remained unaltered in the aged dKI mice (Fig. 4, *I* and *J*), suggesting that A $\beta$ -amyloidosis does not directly affect alternative splicing of the tau gene.

## Humanization of murine *Mapt* gene

We previously observed no atrophy in these regions in aged *App<sup>NL-G-F</sup>/MAPT* dKI mice from 18 to 24 months and detected only a low level of caspase-3 activation in *App<sup>NL-G-F</sup>/MAPT* dKI

mice as well as in *App<sup>NL-G-F</sup>* KI mice (21). These findings indicate that humanization of the *Mapt* gene does not affect neurodegenerative processes in these mouse models of extensive A $\beta$ -amyloidosis.



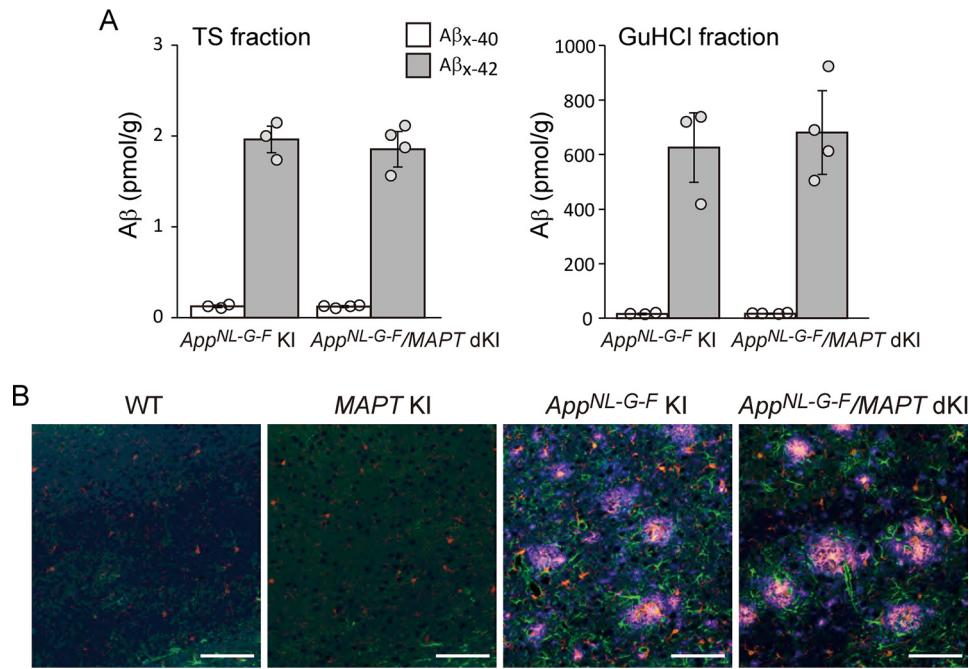


**Figure 3. Amyloid deposition and neuroinflammation in 6-month-old *App<sup>NL-G-F</sup>/MAPT dKI* mice.** *A*, biochemical quantification of A $\beta$  in mouse brains. A $\beta_{40}$  and A $\beta_{42}$  in the TS and GuHCl fractions of cortical tissue from 6-month-old mouse brains were quantified by sandwich ELISA. Data represent mean  $\pm$  S.E. (error bars) ( $n = 3$  (*App<sup>NL-G-F</sup> KI*) and  $n = 4$  (*App<sup>NL-G-F</sup>/MAPT dKI*), Student's *t* test (TS-A $\beta_{40}$ :  $t(5) = 0.168$ ,  $p = 0.563$ ; TS-A $\beta_{42}$ :  $t(5) = 0.408$ ,  $p = 0.650$ ; GuHCl-A $\beta_{40}$ :  $t(5) = 0.377$ ,  $p = 0.361$ ; GuHCl-A $\beta_{42}$ :  $t(5) = 0.419$ ,  $p = 0.346$ ). *B*, amyloid depositions and neuroinflammation were detected by triple staining of brains from 6-month-old mice using anti-A $\beta$ 1-x antibody (82E1) (blue), anti-GFAP antibody (green), and anti-Iba1 antibody (red) as markers of A $\beta$  plaque, astrocytosis, and microgliosis, respectively. Scale bars, 100  $\mu$ m.

**Propagation of AD brain-derived pathological tau proteins in WT, *App KI*, *MAPT KI*, and *App<sup>NL-G-F</sup>/MAPT dKI* mice**

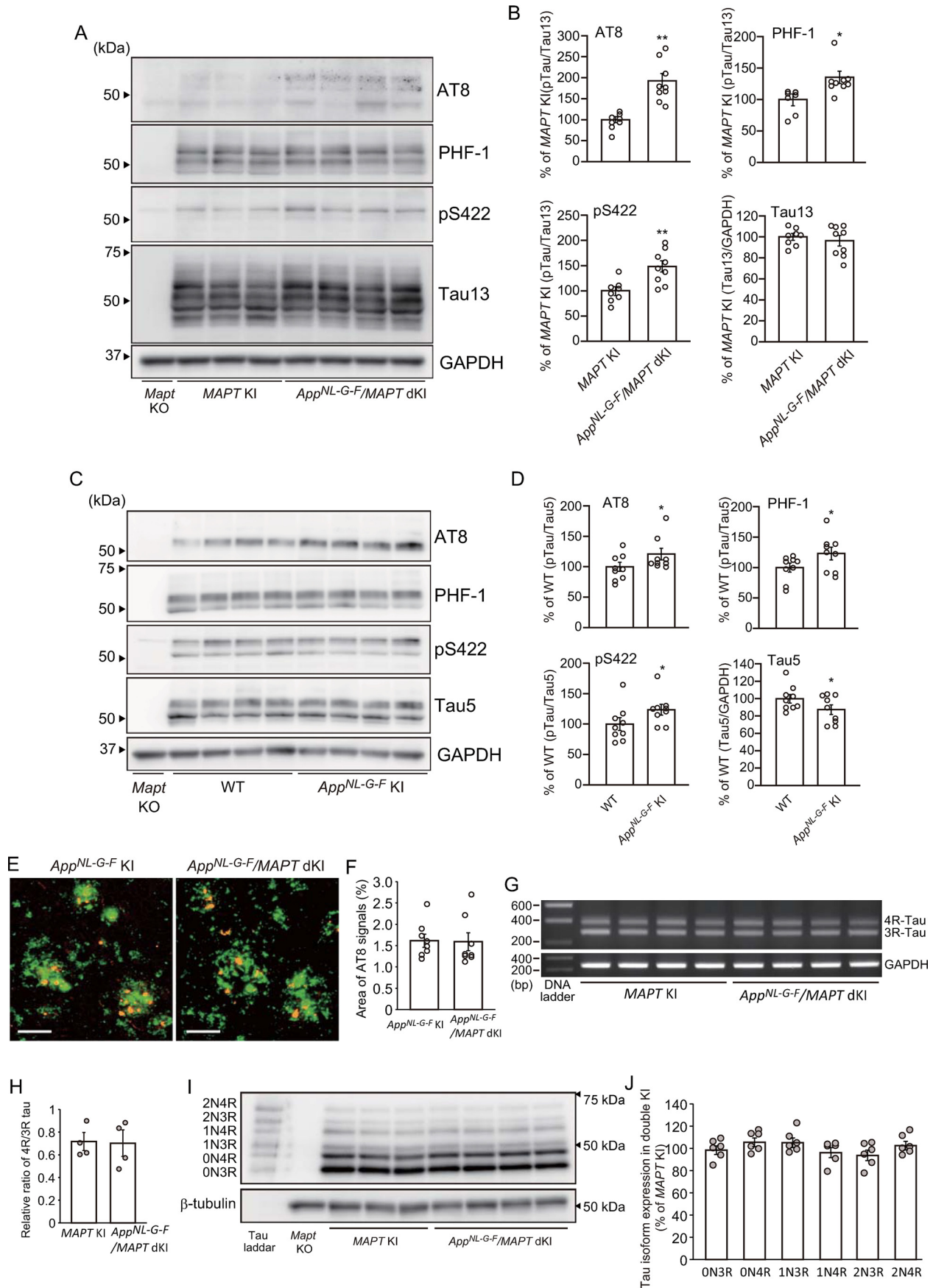
Propagation of pathological proteins associated with neurodegeneration, such as tau, A $\beta$ ,  $\alpha$ -synuclein, and TDP-43, has been shown to represent the primary mechanism that accounts for progressive spreading of pathogenic agents (26). Based on the experimental paradigm described previously (13), we analyzed whether humanization of murine tau protein affects pathological tau propagation in WT and *App KI* mouse brains (Fig. 6).

The first notable observation is that humanization of murine tau in WT mice boosted propagation of AD brain-derived pathological tau (Fig. 6*A*, left panels), indicating that humanization of the host animal tau affects the transmission of the pathogenic agents. In addition, the presence of A $\beta$  plaques augmented tau pathology seeded by the AD brain-derived pathological tau proteins in single *App<sup>NL-G-F</sup> KI* mice (Fig. 6, *A* and *B*) in agreement with the previous report (13). Of particular note, *App<sup>NL-G-F</sup>/MAPT dKI* mice exhibited greater pathological propagation than *App<sup>NL-G-F</sup> KI* mice (Fig. 6, *A* and *B*). In addition, we observed many more AT8-positive tau aggregates in dystrophic neurites surrounding A $\beta$  plaques in *App<sup>NL-G-F</sup>/MAPT dKI* than single *App<sup>NL-G-F</sup> KI* mice (Fig. 6, *C* and *D*), but

we did not detect thioflavin S- or Gallyas silver-positive NFT formation (data not shown). These differences between WT and *MAPT KI* mice or *App KI* and *App KI/MAPT dKI* mice were undetectable unless the AD brain-derived pathological tau was introduced. Our findings probably imply that there exists a species preference (*i.e.* mice versus humans) in the dynamic interactions between the pathological and normal tau proteins. This may possibly apply to some other pathogenic proteins, such as  $\alpha$ -synuclein, associated with neurodegenerative diseases.

The experimental inoculation of the pathological tau protein derived from AD brain, however, did not evoke NFT formation or neurodegeneration in *App<sup>NL-G-F</sup>/MAPT dKI* mice. These findings suggest that tau propagation in dystrophic neurites is likely an initial stage of tau pathology formation and neurodegeneration, which proceeds over decades in human brains (12). Because many of the pathogenic mutations in the *MAPT* gene that cause FTDP-17 are located in the genomic regions corresponding to microtubule-binding domains (27) and because some mutations in the exon 10-intron 10 interface are also pathogenic by affecting alternative splicing (27), introduction of these mutations into the human *MAPT KI* mice may lead to a generation of relevant tauopathy models by accelerating the

**Figure 2. Pathological changes in 6-month-old of *App<sup>NL-G-F</sup>/MAPT dKI* mice.** *A* and *B*, status of tau phosphorylation in 6-month-old single *MAPT KI* and *App<sup>NL-G-F</sup>/MAPT dKI* mice was immunoblotted with the anti-tau antibodies AT8, PHF-1, pS422, and Tau13. Data represent mean  $\pm$  S.E. ( $n = 8$  (*MAPT KI*) and  $n = 8$  (*App<sup>NL-G-F</sup>/MAPT dKI*), Student's *t* test (AT8:  $t(14) = 5.853$  (\*\*,  $p = 2.1 \times 10^{-3}$ ); PHF-1:  $t(14) = 2.551$  (\*,  $p = 0.012$ ); pS422:  $t(14) = 3.758$  (\*\*,  $p = 0.001$ ); Tau13:  $t(14) = 1.165$ ,  $p = 0.868$ ). *C* and *D*, status of tau phosphorylation in 6-month-old single *App<sup>NL-G-F</sup> KI* mice. Data represent mean  $\pm$  S.E. ( $n = 7$  (WT) and  $n = 7$  (*App<sup>NL-G-F</sup> KI*)); \*,  $p < 0.05$ , Student's *t* test (AT8:  $t(12) = 2.500$  (\*,  $p = 0.014$ ); PHF-1:  $t(12) = 6.464$  (\*\*,  $p = 1.55 \times 10^{-3}$ ); pS422:  $t(12) = 2.584$  (\*,  $p = 0.012$ ); Tau5:  $t(12) = 2.656$  ( $p = 0.07$ )). *E* and *F*, immunostaining of pathological tau in mouse brains. Brain sections were immunostained with the anti-A $\beta$  antibody, A $\beta_{1-x}$  (green), and AT8 (red). Scale bars, 50  $\mu$ m. Data represent mean  $\pm$  S.E. (error bars) ( $n = 8$  (*App<sup>NL-G-F</sup> KI*) and  $n = 9$  (*App<sup>NL-G-F</sup>/MAPT dKI*), where each *n* reflects one mouse (with four 4- $\mu$ m sections averaged to a single value per mouse)); Student's *t* test (AT8:  $t(15) = 0.050$ ,  $p = 0.481$ ).



## Humanization of murine *Mapt* gene

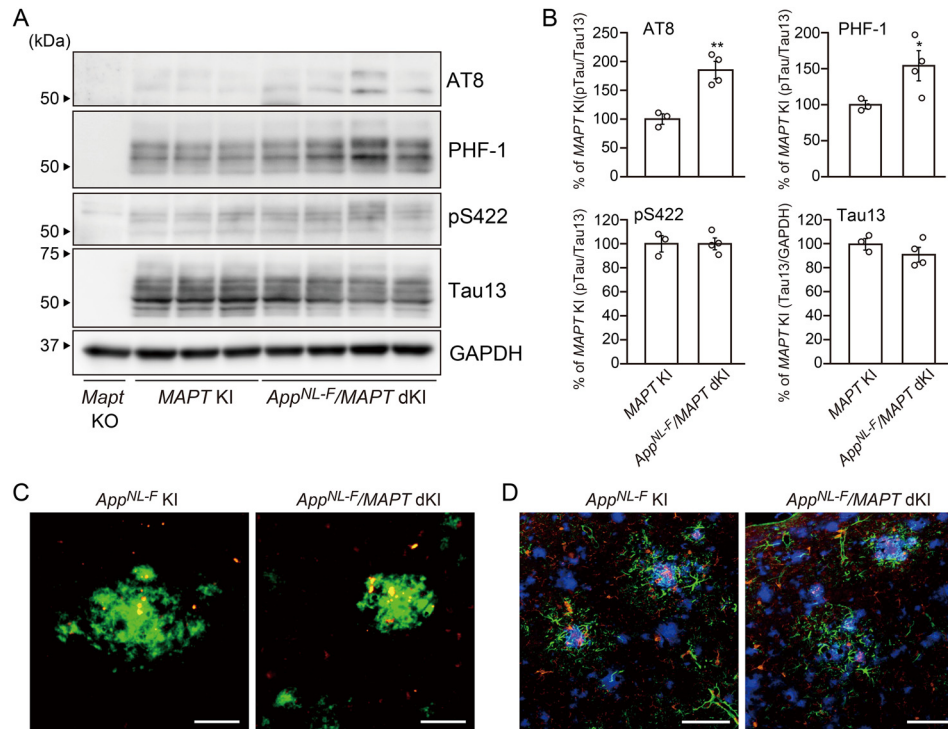


**Figure 5. Amyloid deposition and neuroinflammation in 24-month-old *App<sup>NL-F</sup>/MAPT dKI* mice.** *A* and *B*, status of tau phosphorylation in 24-month-old single *MAPT KI* and *App<sup>NL-F</sup>/MAPT dKI* mice was immunoblotted with the anti-tau antibodies AT8, PHF-1, pS422, and Tau13. Data represent mean  $\pm$  S.E. (error bars) ( $n = 3$  (*MAPT KI*) and  $n = 4$  (*App<sup>NL-F</sup>/MAPT dKI*)), Student's *t* test (AT8:  $t(5) = 5.108$  (\*\*,  $p = 0.0019$ ); PHF-1:  $t(5) = 2.473$  (\*,  $p = 0.028$ ); pS422:  $t(5) = 0.004$ ,  $p = 0.501$ ; Tau13:  $t(5) = 1.220$ ,  $p = 0.861$ )). *C*, immunostaining of pathological tau in 24-month-old *App<sup>NL-F</sup>/MAPT dKI* mouse brains. Brain sections were immunostained with  $A\beta_{1-x}$  (green) and AT8 (red). *D*, amyloid depositions and neuroinflammation were detected by triple staining of 24-month-old mice using 82E1 (blue), anti-GFAP antibody (green), and anti-Iba1 antibody (red) as markers of  $A\beta$  plaque, astrocytosis, and microgliosis, respectively. Scale bars, 50  $\mu\text{m}$  (*C*) and 100  $\mu\text{m}$  (*D*).

pathological processes without depending on the overexpression paradigm.

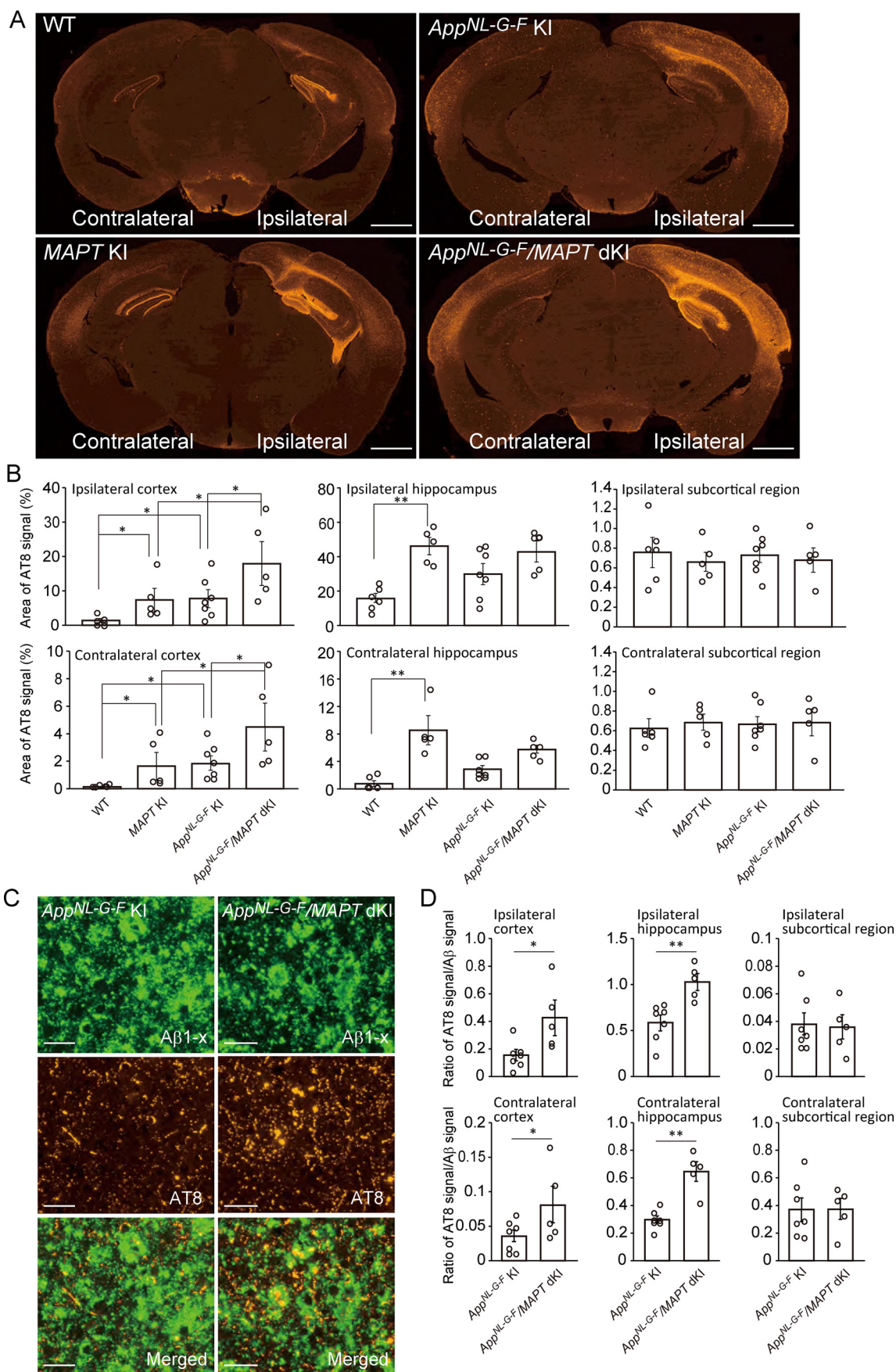
### Discussion

Human tau and murine tau differ from each other not only in terms of their primary structure but also in their isoform profile created by alternative splicing (17). There are six isoforms of tau in adult human brain and three isoforms in murine brain. This probably explains why humanization of murine tau resulted in enhanced propagation of pathological human tau not only in the absence but also in the presence of  $A\beta$ -amyloidosis. Our results indicate that humanization of the murine *Mapt* gene exerts little effect, if any, on the physiological and pathological parameters of WT and single *App KI* mouse models of preclinical AD (7). This indicates that the humanization of murine tau does not artificially perturb the structure and function of mouse brain and thus makes the *MAPT KI* mouse an ideal platform

from which to study different forms of tauopathy, including FTDP-17. In this way, the transgenic overexpression paradigm, which may abolish endogenous gene loci and/or induce artificial phenotypes can be avoided (7, 28).

The *MAPT KI* mouse model can be applied to the study of neurodegenerative diseases involving tauopathy in a number of ways. For instance, the mice would be a useful tool for investigating the molecular mechanisms underlying pathogenesis of Pick's disease, as the *MAPT KI* mice exhibited a relatively higher 3R-tau expression (21). This is because the 3R-tau aggregates accumulate in the brain of Pick's disease patients (14), whereas the adult mouse brain only expresses 4R-tau. Consistently, some mutations in the *MAPT* gene that affect the alternative splicing cause FTDP-17 (27), making the murine *Mapt* gene a less attractive target for gene manipulation. Thus, introduction of mutations associated with FTDP-17 (27) into the exons and introns of the *MAPT* gene in the *App/MAPT dKI*

**Figure 4. Pathological changes at 24 months old of *App<sup>NL-G-F</sup>/MAPT dKI* mice.** *A* and *B*, status of tau phosphorylation in 24-month-old single *MAPT KI* and *App<sup>NL-G-F</sup>/MAPT dKI* mice were immunoblotted with the anti-tau antibodies, AT8, PHF-1, pS422, and Tau13. Data represent mean  $\pm$  S.E. (error bars) ( $n = 8$  (*MAPT KI*) and  $n = 9$  (*App<sup>NL-G-F</sup>/MAPT dKI*)), Student's *t* test (AT8:  $t(15) = 5.126$  (\*\*,  $p = 6.21 \times 10^{-5}$ ); PHF-1:  $t(15) = 2.999$  (\*\*,  $p = 0.0045$ ); pS422:  $t(15) = 3.521$  (\*\*,  $p = 0.002$ ); Tau13:  $t(15) = 0.637$  ( $p = 0.733$ )). *C* and *D*, phosphorylation of murine tau in 24-month-old single *App<sup>NL-G-F</sup> KI* mice. Data represent mean  $\pm$  S.E. ( $n = 3$  (WT) and  $n = 4$  (*App<sup>NL-G-F</sup> KI*)) (\*\*,  $p < 0.01$ ), Student's *t* test (AT8:  $t(5) = 4.239$ ,  $p = 0.0041$ ; PHF-1:  $t(5) = 3.396$ ,  $p = 0.0097$ ; pS422:  $t(5) = 1.572$ ,  $p = 0.912$ ; Tau5:  $t(5) = 1.220$ ,  $p = 0.861$ )). *E* and *F*, immunostaining of pathological tau in mouse brains. Brain sections were immunostained with  $A\beta_{1-x}$  (green), and AT8 (red). Scale bars, 50  $\mu\text{m}$ . Data represent mean  $\pm$  S.E. ( $n = 8$  (*App<sup>NL-G-F</sup> KI*) and  $n = 8$  (*App<sup>NL-G-F</sup>/MAPT dKI*)), where each *n* reflects one mouse (with four 4- $\mu\text{m}$  sections averaged to a single value per mouse); Student's *t* test (AT8:  $t(14) = 0.095$ ,  $p = 0.537$ ). *G* and *H*, the relative ratio of 4R-tau/3R-tau in aged mice was calculated by semiquantitative RT-PCR. Data represent mean  $\pm$  S.E. ( $n = 4$  each; Student's *t* test:  $t(6) = 0.122$ ,  $p = 0.547$ ). *I* and *J*, Tau isoforms in aged *App<sup>NL-G-F</sup>/MAPT dKI* mouse brains. Dephosphorylated biochemical extracts of the brains were subjected to Western blot analysis using Tau13. The relative expression of tau isoforms in *App<sup>NL-G-F</sup>/MAPT dKI* mouse brains was calculated by densitometric analysis. Data represent mean  $\pm$  S.E. ( $n = 5$  (*MAPT KI*) and  $n = 6$  (*App<sup>NL-G-F</sup>/MAPT dKI*)); Student's *t* test (0N3R:  $t(9) = 0.211$ ,  $p = 0.581$ ; 0N4R:  $t(9) = 1.157$ ,  $p = 0.139$ ; 1N3R:  $t(9) = 1.146$ ,  $p = 0.141$ ; 1N4R:  $t(9) = 0.522$ ,  $p = 0.693$ ; 2N3R:  $t(9) = 0.897$ ,  $p = 0.803$ ; 2N4R:  $t(9) = 0.407$ ,  $p = 0.347$ )).



## Humanization of murine *Mapt* gene

mice by genome editing (15) may lead to generation of a pertinent model of AD if the mutations in the coding regions of the *MAPT* gene mimic the pathogenic effect of tau hyperphosphorylation, which may contribute to detachment of the microtubule-bound tau. On the other hand, the molecular mechanisms underlying pathogenesis of four-repeat tauopathy (e.g. progressive supranuclear palsy or corticobasal degeneration) are still elusive (14). Despite such patients also expressing three-repeat tau, only four-repeat tau forms aggregate at a specific region in the brains of patients with the diseases. For further investigation, the *MAPT* KI mice would be needed.

Many of the tau propagation studies to date have used transgenic mice overexpressing mutant human tau protein (29). We have shown here that the pathological tau protein from AD brain interacts better with human tau than with murine tau *in vivo*. This may signify that the presence of murine tau slows human tau-seeded tau propagation in the brain. Thus, humanized tau models with/without A $\beta$ -amyloidosis are advantageous resources for the study of pathological tau propagation. Tau protein resembles prion protein in its ability to propagate (30). The common underlying mechanisms likely involve conformational changes caused by the pathogenic forms as templates (31). Propagation of prion, however, is generally much faster than that of tau (31), presumably because prion protein is a glycosylphosphatidylinositol-anchored protein with  $\beta$ -sheet structure unlike tau protein (32).

The *App/MAPT* dKI mice showed a higher tau phosphorylation status than the single *MAPT* KI mice but lacked apparent tauopathy and neurodegeneration, in a manner essentially identical to that of single *App* KI mice, despite massive A $\beta$  pathology and neuroinflammation. These observations, consistent with the chronology of clinical AD, in which A $\beta$ -amyloidosis precedes tauopathy and neurodegeneration by more than a decade, imply the presence of mechanism(s) that protect the brain from tauopathy and neurodegeneration. Aggravating A $\beta$  plaque-associated factors may also exist that promote tauopathy and neurodegeneration. The balance between aggravating and protective factors may determine the timing of subsequent pathological events, meaning that identifying such factors may open new approaches for the development of preventive medications for neurodegenerative diseases.

Whereas the disease specificity of tauopathy is relatively broad, that of A $\beta$ -amyloidosis is narrow (33), implying that the causal and mechanistic specificity of the former is broader than that of the latter. Bearing in mind that essentially all familial AD mutations cause both A $\beta$ -amyloidosis and tauopathy (34), we propose that long-term pathological stresses caused by A $\beta$ -am-

yloidosis, neuroinflammation, etc. could induce the kinetic changes represented by the liquid–liquid phase separation (LLPS) of tau (35). Recently, Boyko *et al.* (36) demonstrated that tau LLPS was largely regulated by intermolecular electrostatic interactions of tau between negatively charged N terminus and positively charged middle/C terminus, and various posttranslational modification of tau could modulate tau LLPS. Although the amino acid sequence of middle to C terminus of murine tau is identical to human tau, the N terminus of murine tau is relatively different from human tau, suggesting that difference of N-terminal motif of tau between murine and human might cause tau LLPS-related species preference of tau (37).

Taken together, our results indicate that human tau protein expressed in the mouse brain plays physiological and pathological roles that are essentially identical to those of murine tau, as the tau humanization did not cause any artificial phenotypes in these mice. At the same time, tau humanization led to significantly amplified interaction between the AD brain-derived pathological tau and normal tau residing in the host brain, indicating that human and murine tau proteins are not 100% identical to each other in pathological terms, whereas their physiological properties are essentially indistinguishable. On the basis of these facts and assumptions, we propose that single *MAPT* KI mice as well as *App/MAPT* dKI mice should serve as useful models for further elucidating the molecular mechanisms underlying the pathogenesis of tauopathies represented by AD and for performing preclinical studies of these disorders accompanying tau pathology.

## Experimental procedures

### Mutant mice

*App*<sup>NL-G-F</sup> mice, which include the Swedish, Arctic, and Iberian mutations, and *MAPT* KI mice were maintained as described previously (5, 21). P301S-tau transgenic mice (PS19) were described previously (22) and then backcrossed to C57BL/6J mice. Tau-deficient mice were obtained from the Jackson Laboratory (stock no. 007251). All mice used in the experiments were on the C57BL/6J background. We used the male mice for the 6-month-old analysis and the female mice for 24-month-old analysis in the present study. All animal experiments were carried out according to the RIKEN Brain Science Institute's guidelines for animal experimentation.

### ELISA of A $\beta$

Soluble materials from mouse cortical hemispheres were dissolved in Tris-HCl-buffered saline (TS fraction) and insoluble materials in guanidine HCl solution (GuHCl fraction) as

**Figure 6. Propagation of AD brain-derived pathological tau in mouse brains.** A and B, immunostaining of pathological tau in mouse brains. Brain sections were immunostained with AT8 (red). Scale bars, 1 mm. The area of AT8 signal in the mice was quantified by image analysis. Data represent mean  $\pm$  S.E. (error bars) ( $n = 6$  (WT),  $n = 7$  (*App*<sup>NL-G-F</sup> KI),  $n = 5$  (*MAPT* KI), and  $n = 5$  (*App*<sup>NL-G-F</sup>/*MAPT* dKI), where each  $n$  reflects one mouse (with four 4- $\mu$ m sections averaged to a single value per mouse); two-way ANOVA with post hoc Scheffe's  $F$  test (ipsilateral of cortex:  $F(1,22) = 5.94$  (\*,  $p = 0.025$ ); ipsilateral of hippocampus:  $F(1,22) = 18.42$  (\*\*,  $p = 0.0004$ ); ipsilateral of subcortical region:  $F(1,22) = 0.474$  ( $p = 0.499$ ); contralateral of cortex:  $F(1,22) = 5.82$  (\*,  $p = 0.026$ ); contralateral of hippocampus:  $F(1,22) = 30.93$  (\*\*,  $p = 2.3 \times 10^{-5}$ ); contralateral of subcortical region:  $F(1,22) = 0.164$  ( $p = 0.690$ )). C and D, immunostaining of pathological tau in mouse brains. Brain sections were immunostained with A $\beta$ <sub>1-x</sub> (green) and AT8 (red). Contralateral cortex images were shown in C. Scale bars, 50  $\mu$ m. The ratio of AT8 signal/A $\beta$ <sub>1-x</sub> signal was calculated by image analysis. Data represent mean  $\pm$  S.E. ( $n = 7$  (*App*<sup>NL-G-F</sup> KI) and  $n = 5$  (*App*<sup>NL-G-F</sup>/*MAPT* dKI), where each  $n$  reflects one mouse (with four 4- $\mu$ m sections averaged to a single value per mouse); Student's  $t$  test (ipsilateral of cortex:  $t(10) = 2.558$  (\*,  $p = 0.014$ ); ipsilateral of hippocampus:  $t(10) = 3.866$  (\*\*,  $p = 0.002$ ); ipsilateral of subcortical region:  $t(10) = 0.192$  ( $p = 0.574$ ); contralateral of cortex:  $t(10) = 1.971$  (\*,  $p = 0.039$ ); contralateral of hippocampus:  $t(10) = 5.722$  (\*\*,  $p = 9.6 \times 10^{-5}$ ); contralateral of subcortical region:  $t(10) = 0.009$  ( $p = 0.497$ )). After injection of human brain-derived pathological tau, some of the mice died as follows: 2 of 8 WT mice; 3 of 8 *MAPT* KI mice; 1 of 8 *App*<sup>NL-G-F</sup> KI mice; 2 of 7 *App*<sup>NL-G-F</sup>/*MAPT* dKI mice.

described previously (38).  $A\beta_{X-40}$  and  $A\beta_{X-42}$  levels in brain extracts were quantified using an  $A\beta$  ELISA kit (Wako, Tokyo, Japan) according to the manufacturer's instructions.  $A\beta_{X-40}$  and  $A\beta_{X-42}$  carrying the Arctic mutation were quantified based on standard curves using synthetic human Arctic  $A\beta$  peptides (Peptide Institute, Osaka, Japan) as described previously (5).

### Western blot analysis of tau

The cortical brain tissue samples were homogenized in lysis buffer (50 mM Tris-HCl (pH 8.0) containing 150 mM NaCl, 50 mM EDTA, 1% Triton X-100, and protease/phosphatase inhibitor mixture) and centrifuged at  $20,000 \times g$  for 20 min at 4 °C, as described previously (39). Brain extracts as the total fraction (15  $\mu$ g of protein/lane) were subjected to Western blotting using anti-Tau antibodies (both mouse and human tau-specific antibody, Tau5 (catalog no. AHB0042, Thermo Fisher Scientific; epitope: amino acid residues 210–214 on the longest isoform of human tau); human tau-specific antibody, Tau13 (catalog no. sc-21796, Santa Cruz Biotechnology, Inc.; epitope: amino acid residues 2–18 on the longest isoform of human tau); 3R-tau-specific antibody, RD3 (catalog no. 05-803, Merck Millipore; epitope: a junction-flanking sequence coded by adjacent exons 9 and 11 in the absence of exon 10); 4R-tau-specific antibody, RD4 (catalog no. MBS604301, MyBiosource, San Diego, CA; epitope: a junction-flanking sequence coded by adjacent exons 9 and 10 of Tau)), anti-phospho-Tau antibodies (AT8 (catalog no. 90206, Innogenetics, Ghent, Belgium; epitope: phosphorylated serine 202 and threonine 205); PHF-1 (kindly provided from Peter Davies, Albert Einstein College of Medicine; epitope: phosphorylated serine 396 and 404); pS422 (catalog no. ab62639, Abcam, Cambridge, UK; epitope: phosphorylated serine 422)), and internal controls (anti- $\beta$ -tubulin antibody (catalog no. ab11312, Abcam) and anti-GAPDH antibody (catalog no. 2275-PC-100, TREVIGEN, Gaithersburg, MD)). To show the specificity of antibodies, brain extract derived from Tau-KO mice was used as a negative control. For analysis of the isoform pattern of tau, brain extracts were dephosphorylated with  $\lambda$ -phosphatase (catalog no. sc-200312A, Santa Cruz Biotechnology) according to the manufacturer's instructions. All six isoforms of human Tau ladder were purchased from rPeptide. Each set of experiments was repeated at least three times to confirm the results. Band intensity was determined with a LAS4000 densitometer (Fujifilm, Tokyo, Japan).

### Immunohistochemical studies

Paraffin-embedded sections were immunostained using antibodies specific to the N termini of  $A\beta$  ( $A\beta_{1-x}$ ) (40) and 82E1 (catalog no. 10323, IBL, Gunma, Japan), to Iba1 (Wako), to GFAP (catalog no. MAB3402, Merck Millipore, Darmstadt, Germany), to tau (pan-tau-specific antibody, Tau1 (catalog no. MAB3420, Merck Millipore, Darmstadt, Germany); murine tau-specific antibody, T49 (catalog no. MABN827, Merck Millipore), Tau5, Tau13), to phosphorylated tau (AT8), and to MAP2 as a dendritic marker (catalog no. M121, Leinco Technologies, St. Louis, MO). To show the specificity of antibodies, brain sections derived from Tau-KO mice were used as a negative control. When necessary, tyramide signal amplification (PerkinElmer Life Sciences) was used as described previously

(41). We performed antigen retrieval by autoclave (121 °C for 5 min).

We quantified the immunoreactive areas using MetaMorph imaging software (Universal Imaging Corp., West Chester, PA) as described previously (41). To reduce the variation of results across tissue sections, we used the average of data from at least four sections per mouse.

### RNA extraction and semiquantitative RT-PCR

Total RNA was extracted from brain samples using RNAiso Plus (Takara, Shiga, Japan) according to the manufacturer's instructions. We performed semiquantitative RT-PCR for detection of both 3R- and 4R-tau mRNA as described previously (42) with minor modifications. The primer pair used for tau was 5'-AAGTCGCCGTCTTCGCAAG-3' and 5'-GTC-CAGGGACCCAATCTTCGA-3', and that for GAPDH was 5'-CCATGGCACCGTCAAGGCTGA-3' and 5'-GCCAGTAGAGGCAGGGATGAT-3'. PCR products of 288 and 381 bp correspond to 3R-tau and 4R-tau, respectively. RT-PCR products were detected by 24, 26, 28, 30, 32, and 34 PCR cycles to mortgage the linearity of the products, and the result was decided by 26 cycles. Band intensity was calibrated using ImageJ software.

### Tau propagation analysis

AD-tau extracted from an AD patient's brain, as described previously (43), was prepared in the laboratory of V. M. Y. L. and J. Q. T. In this study, AD-tau was provided from the same batch of extracts (43). We injected AD brain-derived tau into the mouse brain by stereotaxic injection as described previously (13, 44). The mice (19-month-old males) were deeply anesthetized and immobilized in a stereotaxic frame (Muromachi). AD brain-derived tau was injected in dorsal hippocampus and overlying cortex in the right hemisphere (bregma:  $-2.5$  mm; lateral  $-2$  mm; depth  $-1.7$  mm and  $-0.5$  mm from brain surface) with a total amount of 2  $\mu$ g of AD-tau using a Hamilton syringe as described (44). After 3 months, we collected the brains, which were fixed in 4% paraformaldehyde, embedded in paraffin, and sectioned into 4- $\mu$ m thickness, as described previously (13), and performed immunohistochemical analysis. Protocols involving the use of human tissue were approved by the Institutional Review Board of the RIKEN Brain Science Institute and University of Pennsylvania, respectively. All of the human materials were taken in accordance with the Declaration of Helsinki.

### AD brain sections

AD brain sections were used as a positive control of tauopathy in all studies. Paraffin-embedded brain (neocortical and hippocampal region) sections from normal humans and AD patients were purchased from Wako. Protocols involving the use of human tissue were approved by the institutional review board of the RIKEN Brain Science Institute.

### Statistics

All data are shown as the mean  $\pm$  S.E. For comparison between two groups, statistical analysis was performed by Student's *t* test. For comparisons among three or more groups,

## Humanization of murine Mapt gene

two-way analysis of variance (ANOVA) or repeated measures ANOVA followed by a post hoc test (Scheffe's *F* test) were used. Normality was tested using Statcel 3 (add-in software for Microsoft Excel). Data were collected and processed in a randomized and blinded manner. No statistical methods were used to predetermine sample size, but our sample sizes are similar to those generally employed in the field.

**Author contributions**—T. S., T. C. S., V. M. Y. L., and J. Q. T. designed this study and wrote the manuscript. T. S., Y. M., and N. M. performed animal experiments. S. N., B. Z., V. M. Y. L., and J. Q. T. provided AD brain-derived pathological tau and jointly discussed the results. S. M. provided human brain tissues. T. S., H. S., S. H., M. H., and T. C. S. jointly analyzed the data.

**Acknowledgments**—We thank Yoshitsugu Shitaka, Mitsuyuki Matsu-moto, Yasuyuki Mitani, Hiroshi Yamada, Shinichi Miyake Mayuko Okabe, Mayako Yamazaki, and Ni Keni (Astellas Pharma, Inc., Tokyo, Japan) for valuable discussion. We also thank Naoko Kamano and Mika Takahashi (RIKEN Center for Brain Science) for technical assistance. We are grateful to the RIKEN Center for Brain Science Research Resource Division for technical support in breeding of the mice. We also thank Per Nilsson (Karolinska Institute) and Kaori Tsukakoshi (Tokyo University of Agriculture and Technology) for valuable discussion. We also thank Maho Morishima (Tokyo Metropolitan Geriatric Hospital) for coordinating brain materials. Naruhiko Sahara (National Institutes for Quantum and Radiological Science and Technology, Chiba, Japan) provided helpful suggestions.

### References

1. Bateman, R. J., Xiong, C., Benzinger, T. L., Fagan, A. M., Goate, A., Fox, N. C., Marcus, D. S., Cairns, N. J., Xie, X., Blazey, T. M., Holtzman, D. M., Santacruz, A., Buckles, V., Oliver, A., Moulder, K., *et al.* (2012) Clinical and biomarker changes in dominantly inherited Alzheimer's disease. *N. Engl. J. Med.* **367**, 795–804 [CrossRef Medline](#)
2. Selkoe, D. J., and Hardy, J. (2016) The amyloid hypothesis of Alzheimer's disease at 25 years. *EMBO Mol. Med.* **8**, 595–608 [CrossRef Medline](#)
3. Robinson, J. L., Lee, E. B., Xie, S. X., Rennert, L., Suh, E., Bredenberg, C., Caswell, C., Van Deerlin, V. M., Yan, N., Yousef, A., Hurtig, H. I., Siderowf, A., Grossman, M., McMillan, C. T., Miller, B., *et al.* (2018) Neurodegenerative disease concomitant proteinopathies are prevalent, age-related and APOE4-associated. *Brain* **141**, 2181–2193 [CrossRef Medline](#)
4. Higuchi, M., Iwata, N., Matsuba, Y., Takano, J., Suemoto, T., Maeda, J., Ji, B., Ono, M., Staufenbiel, M., Suhara, T., and Saido, T. C. (2012) Mechanistic involvement of the calpain-calpastatin system in Alzheimer neuropathology. *FASEB J.* **26**, 1204–1217 [CrossRef Medline](#)
5. Saito, T., Matsuba, Y., Mihira, N., Takano, J., Nilsson, P., Itohara, S., Iwata, N., and Saido, T. C. (2014) Single App knock-in mouse models of Alzheimer's disease. *Nat. Neurosci.* **17**, 661–663 [CrossRef Medline](#)
6. Saito, T., Matsuba, Y., Yamazaki, N., Hashimoto, S., and Saido, T. C. (2016) Calpain activation in Alzheimer's model mice is an artifact of APP and presenilin overexpression. *J. Neurosci.* **36**, 9933–9936 [CrossRef Medline](#)
7. Sasaguri, H., Nilsson, P., Hashimoto, S., Nagata, K., Saito, T., De Strooper, B., Hardy, J., Vassar, R., Winblad, B., and Saido, T. C. (2017) APP mouse models for Alzheimer's disease preclinical studies. *EMBO J.* **36**, 2473–2487 [CrossRef Medline](#)
8. Goedert, M., Spillantini, M. G., Jakes, R., Rutherford, D., and Crowther, R. A. (1989) Multiple isoforms of human microtubule-associated protein tau: sequences and localization in neurofibrillary tangles of Alzheimer's disease. *Neuron* **3**, 519–526 [CrossRef Medline](#)
9. Götz, J., Probst, A., Spillantini, M. G., Schäfer, T., Jakes, R., Bürki, K., and Goedert, M. (1995) Somatodendritic localization and hyperphosphorylation of tau protein in transgenic mice expressing the longest human brain tau isoform. *EMBO J.* **14**, 1304–1313 [CrossRef Medline](#)
10. Kubo, A., Misonou, H., Matsuyama, M., Nomori, A., Wada-Kakuda, S., Takashima, A., Kawata, M., Murayama, S., Ihara, Y., and Miyasaka, T. (2019) Distribution of endogenous normal tau in the mouse brain. *J. Comp. Neurol.* **527**, 985–998 [CrossRef Medline](#)
11. Spillantini, M. G., and Goedert, M. (2013) Tau pathology and neurodegeneration. *Lancet Neurol.* **12**, 609–622 [CrossRef Medline](#)
12. Braak, H., and Braak, E. (1991) Neuropathological staging of Alzheimer-related changes. *Acta Neuropathol.* **82**, 239–259 [CrossRef Medline](#)
13. He, Z., Guo, J. L., McBride, J. D., Narasimhan, S., Kim, H., Changolkar, L., Zhang, B., Gathagan, R. J., Yue, C., Dengler, C., Stieber, A., Nitla, M., Coulter, D. A., Abel, T., Brunden, K. R., *et al.* (2018) Amyloid- $\beta$  plaques enhance Alzheimer's brain tau-seeded pathologies by facilitating neuritic plaque tau aggregation. *Nat. Med.* **24**, 29–38 [CrossRef Medline](#)
14. Buée, L., Bussièrè, T., Buée-Scherrer, V., Delacourte, A., and Hof, P. R. (2000) Tau protein isoforms, phosphorylation and role in neurodegenerative disorders. *Brain Res. Brain Res. Rev.* **33**, 95–130 [CrossRef Medline](#)
15. Sasaguri, H., Nagata, K., Sekiguchi, M., Fujioka, R., Matsuba, Y., Hashimoto, S., Sato, K., Kurup, D., Yokota, T., and Saido, T. C. (2018) Introduction of pathogenic mutations into the mouse Psen1 gene by Base Editor and Target-AID. *Nat. Commun.* **9**, 2892 [CrossRef Medline](#)
16. Hong, M., Zhukareva, V., Vogelsberg-Ragaglia, V., Wszolek, Z., Reed, L., Miller, B. L., Geschwind, D. H., Bird, T. D., McKeel, D., Goate, A., Morris, J. C., Wilhelmsen, K. C., Schellenberg, G. D., Trojanowski, J. Q., and Lee, V. M. (1998) Mutation-specific functional impairments in distinct tau isoforms of hereditary FTDP-17. *Science* **282**, 1914–1917 [CrossRef Medline](#)
17. Andreadis, A. (2005) Tau gene alternative splicing: expression patterns, regulation and modulation of function in normal brain and neurodegenerative diseases. *Biochim. Biophys. Acta* **1739**, 91–103 [CrossRef Medline](#)
18. Jankowsky, J. L., and Zheng, H. (2017) Practical considerations for choosing a mouse model of Alzheimer's disease. *Mol. Neurodegener.* **12**, 89 [CrossRef Medline](#)
19. Ando, K., Leroy, K., Heraud, C., Kabova, A., Yilmaz, Z., Authelat, M., Suain, V., De Decker, R., and Brion, J. P. (2010) Deletion of murine tau gene increases tau aggregation in a human mutant tau transgenic mouse model. *Biochem. Soc. Trans.* **38**, 1001–1005 [CrossRef Medline](#)
20. Chen, Y., Liu, L., Li, M., Yao, E., Hao, J., Dong, Y., Zheng, X., and Liu, X. (2018) Expression of human Tau40 in the medial entorhinal cortex impairs synaptic plasticity and associated cognitive functions in mice. *Biochem. Biophys. Res. Commun.* **496**, 1006–1012 [CrossRef Medline](#)
21. Hashimoto, S., Matsuba, Y., Kamano, N., Mihira, N., Sahara, N., Takano, J., Muramatsu, S. I., Saido, T. C., and Saito, T. (2019) Tau binding protein CAPON induces tau aggregation and neurodegeneration. *Nat. Commun.* **10**, 2394 [CrossRef Medline](#)
22. Yoshiyama, Y., Higuchi, M., Zhang, B., Huang, S. M., Iwata, N., Saido, T. C., Maeda, J., Suhara, T., Trojanowski, J. Q., and Lee, V. M. (2007) Synapse loss and microglial activation precede tangles in a P301S tauopathy mouse model. *Neuron* **53**, 337–351 [CrossRef Medline](#)
23. Hoover, B. R., Reed, M. N., Su, J., Penrod, R. D., Kotilinek, L. A., Grant, M. K., Pitstick, R., Carlson, G. A., Lanier, L. M., Yuan, L. L., Ashe, K. H., and Liao, D. (2010) Tau mislocalization to dendritic spines mediates synaptic dysfunction independently of neurodegeneration. *Neuron* **68**, 1067–1081 [CrossRef Medline](#)
24. Glatz, D. C., Rujescu, D., Tang, Y., Berendt, F. J., Hartmann, A. M., Faltraco, F., Rosenberg, C., Hulette, C., Jellinger, K., Hampel, H., Riederer, P., Möller, H. J., Andreadis, A., Henkel, K., and Stamm, S. (2006) The alternative splicing of tau exon 10 and its regulatory proteins CLK2 and TRA2-BETA1 changes in sporadic Alzheimer's disease. *J. Neurochem.* **96**, 635–644 [CrossRef Medline](#)
25. Schoch, K. M., DeVos, S. L., Miller, R. L., Chun, S. J., Norrbom, M., Wozniak, D. F., Dawson, H. N., Bennett, C. F., Rigo, F., and Miller, T. M. (2016) Increased 4R-Tau induces pathological changes in a human-Tau mouse model. *Neuron* **90**, 941–947 [CrossRef Medline](#)
26. Luk, K. C., Covell, D. J., Kehm, V. M., Zhang, B., Song, I. Y., Byrne, M. D., Pitkin, R. M., Decker, S. C., Trojanowski, J. Q., and Lee, V. M. (2016) Molecular and biological compatibility with host  $\alpha$ -synuclein influences fibril pathogenicity. *Cell Rep.* **16**, 3373–3387 [CrossRef Medline](#)

27. Ghetti, B., Oblak, A. L., Boeve, B. F., Johnson, K. A., Dickerson, B. C., and Goedert, M. (2015) Invited review: frontotemporal dementia caused by microtubule-associated protein tau gene (MAPT) mutations: a chameleon for neuropathology and neuroimaging. *Neuropathol. Appl. Neurobiol.* **41**, 24–46 [CrossRef Medline](#)
28. Goodwin, L. O., Splinter, E., Davis, T. L., Urban, R., He, H., Braun, R. E., Chesler, E. J., Kumar, V., van Min, M., Ndukum, J., Philip, V. M., Reinholdt, L. G., Svenson, K., White, J. K., Sasner, M., Lutz, C., and Murray, S. A. (2019) Large-scale discovery of mouse transgenic integration sites reveals frequent structural variation and insertional mutagenesis. *Genome Res.* **29**, 494–505 [CrossRef Medline](#)
29. Goedert, M., Eisenberg, D. S., and Crowther, R. A. (2017) Propagation of tau aggregates and neurodegeneration. *Annu. Rev. Neurosci.* **40**, 189–210 [CrossRef Medline](#)
30. Kumar, H., and Udgaonkar, J. B. (2019) Mechanistic approaches to understand the prion-like propagation of aggregates of the human tau protein. *Biochim. Biophys. Acta Proteins Proteom.* [CrossRef Medline](#)
31. Vasili, E., Dominguez-Mejide, A., and Outeiro, T. F. (2019) Spreading of  $\alpha$ -synuclein and Tau: a systematic comparison of the mechanisms involved. *Front. Mol. Neurosci.* **12**, 107 [CrossRef Medline](#)
32. Puig, B., Altmepfen, H., and Glatzel, M. (2014) The GPI-anchoring of PrP: implications in sorting and pathogenesis. *Prion* **8**, 11–18 [CrossRef Medline](#)
33. Wolfe, M. S. (2012) The role of tau in neurodegenerative diseases and its potential as a therapeutic target. *Scientifica (Cairo)* **2012**, 796024 [CrossRef Medline](#)
34. Lee, V. M., and Trojanowski, J. Q. (1999) Neurodegenerative tauopathies: human disease and transgenic mouse models. *Neuron* **24**, 507–510 [CrossRef Medline](#)
35. Ambadipudi, S., Biernat, J., Riedel, D., Mandelkow, E., and Zweckstetter, M. (2017) Liquid-liquid phase separation of the microtubule-binding repeats of the Alzheimer-related protein Tau. *Nat. Commun.* **8**, 275 [CrossRef Medline](#)
36. Boyko, S., Qi, X., Chen, T.-H., Surewicz, K., and Surewicz, W. K. (2019) Liquid-liquid phase separation of tau protein: the crucial role of electrostatic interactions. *J. Biol. Chem.* **274**, 11054–11059 [CrossRef Medline](#)
37. Stefanoska, K., Volkerling, A., Bertz, J., Poljak, A., Ke, Y. D., Ittner, L. M., and Ittner, A. (2018) An N-terminal motif unique to primate tau enables differential protein-protein interactions. *J. Biol. Chem.* **293**, 3710–3719 [CrossRef Medline](#)
38. Iwata, N., Mizukami, H., Shirotani, K., Takaki, Y., Muramatsu, S., Lu, B., Gerard, N. P., Gerard, C., Ozawa, K., and Saido, T. C. (2004) Pre-synaptic localization of neprilysin contributes to efficient clearance of amyloid- $\beta$  peptide in mouse brain. *J. Neurosci.* **24**, 991–998 [CrossRef Medline](#)
39. Higuchi, M., Tomioka, M., Takano, J., Shirotani, K., Iwata, N., Masumoto, H., Maki, M., Itohara, S., and Saido, T. C. (2005) Distinct mechanistic roles of calpain and caspase activation in neurodegeneration as revealed in mice overexpressing their specific inhibitors. *J. Biol. Chem.* **280**, 15229–15237 [CrossRef Medline](#)
40. Saido, T. C., Iwatsubo, T., Mann, D. M., Shimada, H., Ihara, Y., and Kawashima, S. (1995) Dominant and differential deposition of distinct  $\beta$ -amyloid peptide species, A $\beta$  N3(pE), in senile plaques. *Neuron* **14**, 457–466 [CrossRef Medline](#)
41. Enya, M., Morishima-Kawashima, M., Yoshimura, M., Shinkai, Y., Kusui, K., Khan, K., Games, D., Schenk, D., Sugihara, S., Yamaguchi, H., and Ihara, Y. (1999) Appearance of sodium dodecyl sulfate-stable amyloid  $\beta$ -protein (A $\beta$ ) dimer in the cortex during aging. *Am. J. Pathol.* **154**, 271–279 [CrossRef Medline](#)
42. Iovino, M., Patani, R., Watts, C., Chandran, S., and Spillantini, M. G. (2010) Human stem cell-derived neurons: a system to study human tau function and dysfunction. *PLoS One* **5**, e13947 [CrossRef Medline](#)
43. Guo, J. L., Narasimhan, S., Changolkar, L., He, Z., Stieber, A., Zhang, B., Gathagan, R. J., Iba, M., McBride, J. D., Trojanowski, J. Q., and Lee, V. M. (2016) Unique pathological tau conformers from Alzheimer's brains transmit tau pathology in nontransgenic mice. *J. Exp. Med.* **213**, 2635–2654 [CrossRef Medline](#)
44. Narasimhan, S., and Lee, V. M. Y. (2017) The use of mouse models to study cell-to-cell transmission of pathological tau. *Methods Cell Biol.* **141**, 287–305 [CrossRef Medline](#)

**Humanization of the entire murine *Mapt* gene provides a murine model of pathological human tau propagation**

Takashi Saito, Naomi Mihira, Yukio Matsuba, Hiroki Sasaguri, Shoko Hashimoto, Sneha Narasimhan, Bin Zhang, Shigeo Murayama, Makoto Higuchi, Virginia M. Y. Lee, John Q. Trojanowski and Takaomi C. Saido

*J. Biol. Chem.* 2019, 294:12754-12765.

doi: 10.1074/jbc.RA119.009487 originally published online July 4, 2019

---

Access the most updated version of this article at doi: [10.1074/jbc.RA119.009487](https://doi.org/10.1074/jbc.RA119.009487)

Alerts:

- [When this article is cited](#)
- [When a correction for this article is posted](#)

[Click here](#) to choose from all of JBC's e-mail alerts

This article cites 44 references, 10 of which can be accessed free at <http://www.jbc.org/content/294/34/12754.full.html#ref-list-1>

## Supporting Information

### **Humanization of the entire murine *Mapt* gene provides a murine model of pathological human tau propagation**

Takashi Saito<sup>1,2\*</sup>, Naomi Mihira<sup>1</sup>, Yukio Matsuba<sup>1</sup>, Hiroki Sasaguri<sup>1</sup>, Shoko Hashimoto<sup>1</sup>, Sneha Narasimhan<sup>3</sup>, Bin Zhang<sup>3</sup>, Shigeo Murayama<sup>4</sup>, Makoto Higuchi<sup>5</sup>, Virginia M.Y. Lee<sup>3</sup>, John Q. Trojanowski<sup>3</sup>, and Takaomi C. Saido<sup>1\*</sup>

<sup>1</sup>Laboratory for Proteolytic Neuroscience, RIKEN Center for Brain Science, 2-1 Hirosawa, Wako-city, Saitama 351-0198, Japan

<sup>2</sup>Department of Neuroscience and Pathobiology, Research Institute of Environmental Medicine, Nagoya University, Nagoya, Aichi 464-8601, Japan

<sup>3</sup>Department of Pathology and Laboratory Medicine, Institute on Aging and Center for Neurodegenerative Disease Research, University of Pennsylvania School of Medicine, Philadelphia, PA 19104, USA

<sup>4</sup>Department of Neuropathology, Tokyo Metropolitan Geriatric Hospital, 35-2 Sakaecho, Itabashi, Tokyo 173-0015, Japan

<sup>5</sup>Department of Functional Brain Imaging Research, National Institute of Radiological Sciences, National Institutes for Quantum and Radiological Science and Technology, Chiba 263-8555, Japan.

#### *Content*

Supplemental Experimental procedure

Supplementary Figure: Figure S1

## Supplemental Experimental procedure

### *Y-maze Test*

The Y-maze test was performed as previously described (5). In this test, each mouse was placed in the center of the maze facing towards one of the arms and then allowed to explore freely for 8 min. The light intensity of the platform was kept constant at 60 lux. We recorded and analyzed the activity and spontaneous behavioral alternations of the mice using Time YM2 for Y-maze software (Two Maze System, O'Hara & Co., Ltd, Japan).

Saito et al. Figure S1

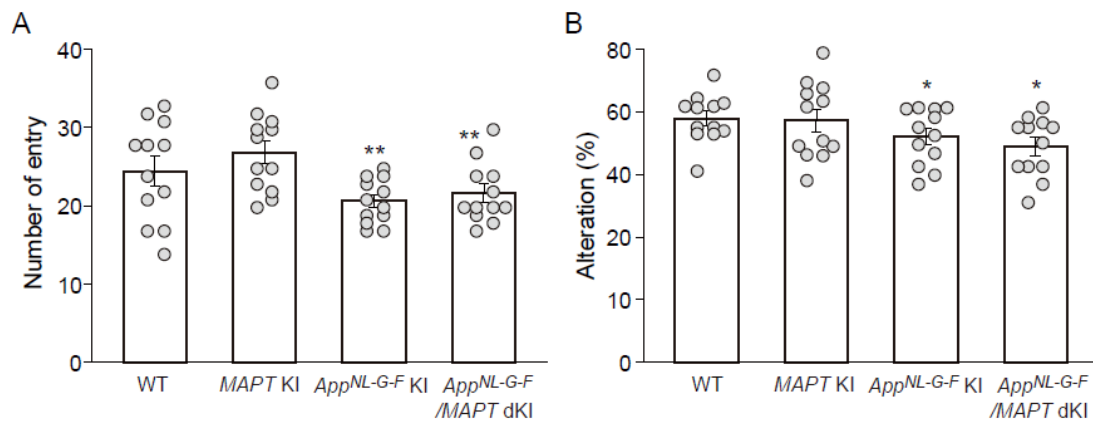


**Figure S1. Memory tests on  $App^{NL-G-F}$  and  $App^{NL-G-F}/MAPT$  KI mice. The Y-maze test was performed on 12-month-old of male mice. A and B, Total entries to the Y-maze arm and the percent alteration were calculated using Time YM2 for Y-maze software (Two Maze System, O'Hara & Co., Ltd, Japan). Data represent mean  $\pm$  SEM (n = 12 each, \* $p < 0.05$ , \*\* $p < 0.01$ ; two-way ANOVA with post-hoc Sheffe's  $F$  test (number of entry:  $F(1,47) = 11.143$ ,  $p = 0.0017$ ; alteration:  $F(1,47) = 6.188$ ,  $p = 0.017$ )).**

Saito et al. Figure S2

